

## AVO analysis using the VSP

**Craig A. Coulombe, Robert R. Stewart, and Michael J. Jones\***

### ABSTRACT

A multioffset VSP geometry and 3-component processing flow have been developed to obtain true reflection coefficients from 3-component VSP data with the purpose of using the reflection coefficients for AVO analysis. The geometry and processing flow have been tested on synthetic data and found to recover the true reflection coefficients for a range of incidence angles. A multioffset field VSP survey was acquired for the analysis of the AVO response of a gas-bearing carbonate. 3-component processing of the data resulted in a good correlation between real and modeled P-P and P-S reflection coefficients. Single interface AVO analysis was found to be inadequate in describing the AVO behavior of the reflections from the top and the base of the gas-bearing carbonate zone, and full multilayer modeling was found to match the real data well.

### INTRODUCTION

Amplitude-variation-with-offset (AVO) analysis has been considered for some time as a useful exploration procedure (Ostrander, 1984; Chacko, 1989; Rutherford and Williams, 1989). The main thrust of AVO analysis is to obtain an estimate of the Poisson's ratio in a subsurface zone using conventional surface seismic data. The principal interest in Poisson's ratio (or equivalently the  $V_p/V_s$  ratio) is that it may be diagnostic of both gas saturation and gross lithology (Tatham and Krug, 1985).

The Knott energy equations (or the Zoeppritz equations) show that the energy reflected from an elastic boundary varies with the angle of incidence of the incident wave (Muskat and Meres, 1940). This behavior was studied further by Koefoed (1955, 1962): He established that the change in reflection coefficient with incident angle is dependent on the Poisson's ratio difference across an elastic boundary. Koefoed (1955) also proposed analyzing the shape of the reflection-coefficient versus angle-of-incidence curve as a method of interpreting lithology. Ostrander (1984) introduced a practical application of the amplitude-variation with incident-angle phenomenon. He used the Zoeppritz amplitude equations (e.g., Aki and Richards, 1980) to analyze the reflection coefficients as a function of the angle of incidence for a simple three-layer, gas-sand model. The model consisted of a sand layer encased in two shale layers. By using published values of Poisson's ratio for shales, brine-saturated sandstones, and gas-saturated sandstones, he determined that there is a significant enough change in reflection coefficient with angle of incidence to discriminate between gas-saturated sandstones and brine-saturated sandstones. He

---

\* Schlumberger of Canada

tested his theoretical observations with real seismic data and determined that AVO could be used as a method of detecting gas sands.

Surface seismic AVO analysis is complicated by many factors relating to the path of the propagating wavefield. Receiver-array attenuation, geometrical spreading, surface-consistent amplitude factors, and absorption are of major importance (Mazzotti and Mirri, 1991). These factors should be considered when processing surface seismic data for AVO analysis. Furthermore, AVO analysis requires an accurate estimation of the P-wave angle of incidence, which is dependent on a good velocity model. Although these factors may be insignificant for most surface seismic applications they may overwhelm a subtle effect such as AVO.

The accuracy of conventional AVO analysis is ultimately tested by the drill bit and borehole measurements. Full waveform sonic measurements can yield  $V_p/V_s$  ratios; however, these measurements are in the 10 to 20 kHz range while seismic measurements are generally in the 5 to 100 Hz range. As shown by Stewart et al. (1984), velocity dispersion can delay VSP traveltimes up to 7.0 ms per 1000 ft (7.0 ms per 305 m). This suggests that modeling seismic AVO responses using sonic velocities may not adequately match surface seismic observations. The VSP may be considered to help alleviate some of the uncertainties associated with correlating surface seismic and sonic log measurements as well as providing a further understanding of AVO. The main advantage of the VSP is that the seismic wavefield is recorded in situ, resulting in a close monitoring of the propagating wavefields.

The objectives of this study are to process 3-component VSP data for true amplitudes and compare the processed amplitudes with theoretical amplitudes.

## VERTICAL SEISMIC PROFILING

The VSP can be used to gain insight into wavefield propagation (Lee and Balch, 1983; Gaiser et al. 1984; and Dankbaar, 1987). There are several aspects of the VSP that can be used to advantage when considering AVO. The downgoing wavefield is recorded, and can be used to design a deconvolution operator that eliminates many of the wavefield propagation effects (such as multiples) between the source and receiver. If we consider the downgoing wavefield in the frequency domain as  $D(\omega)$ , and design an operator,  $O(\omega)$ , which collapses the downgoing wavefield into a desired wavelet  $W(\omega)$ ,

$$D(\omega)O(\omega)=W(\omega).$$

We can solve this equation for the operator as

$$O(\omega)=W(\omega)/D(\omega).$$

Thus the downgoing wavefield can be used to design a deconvolution operator that shapes the downgoing wavefield into a known wavelet. The upgoing wavefield is the downgoing wavefield convolved with the reflection coefficient series of the earth. In the frequency domain this can be expressed as

$$U(\omega)=D(\omega)R(\omega).$$

So, convolving the upgoing wavefield with the operator designed from the downgoing wavefield results in the reflection coefficient series convolved with the desired wavelet

$$O(\omega)U(\omega)=W(\omega)R(\omega),$$

as shown by Gaiser et al. (1984). Additionally, the amplitudes of the seismic wavefield are recorded, and can be used to obtain a good estimate of the reflection coefficient of an interface by taking the ratio of the incident and reflected amplitudes. Reflection coefficients were measured using the VSP many years ago by Jolly (1953). Furthermore, the incident and reflected amplitudes can be measured immediately above the interface, eliminating most wavefield propagation effects.

Another aspect of the VSP is that three-component acquisition and processing can be used to obtain the P-SV reflections and thus the P-SV reflection coefficients. This suggests that both P-P and P-SV reflection coefficient variations with offset can be used to estimate the subsurface rock properties. Therefore, the VSP is a promising method of observing AVO because it is independent of many wavefield propagation effects associated with measuring seismic reflections at large distances from the reflecting interface as in the surface seismic case.

A multioffset (walkaway) geometry (Figure 1) is used to record data specifically for AVO analysis of a particular interface. Several offsets are acquired to obtain the reflection coefficients for a range of P-wave angles of incidence. The wavefield is recorded at several levels in the borehole to accommodate multichannel wavefield separation filters. Recording the wavefield directly above the reflector is a major advantage of the VSP. This receiver geometry reduces the effect of many aspects of wavefield propagation (attenuation, transmission losses, multiples, and spherical spreading), and should yield an accurate measurement of the true reflection amplitude by measuring the ratio of the amplitudes of the incident waves to the reflected waves.

## EXPERIMENT DESIGN AND ACQUISITION

A field VSP survey has been acquired to test the proposed AVO VSP method. The survey consists of three VSP types; a zero-offset VSP, an offset VSP, and a multioffset VSP. The geometry of the survey is shown in Figure 2. All the VSPs were recorded using a single level three component down hole geophone. The source consisted of two Hemi-44 vibrators with an 8 to 90 Hz 16 s linear sweep. The zero-offset VSP consists of 99 levels recorded between depths of 3850 m and 1500 m with a spacing of 25 m. The offset VSP consists of 94 levels recorded between depths of 3825 m and 1500 m with a 25 m level spacing. The multioffset VSP consists of 6 VSPs; 11 levels each recorded between depths of 3825 m and 3575 m with a 25 m level spacing.

## VSP PROCESSING

Each VSP shown in Figure 2 contains different information. All the VSPs yield a true time-to-depth correlation. The arrival times of the P-wave direct arrival from the zero-offset VSP can be used in a traveltime inversion algorithm to obtain the interval P-wave velocities. Similarly the arrival times of the S-wave direct arrival or a

near-surface mode-converted S wave can be used to obtain the shear-wave interval velocities. Thus a good understanding of the P- and S-wave velocities can be obtained from the zero-offset and offset VSPs.

The multioffset (walkaway) VSP has been processed using the flow outlined in Figure 3. The purpose of the processing flow is to recover the true reflection amplitudes from three-component VSP data. The intent is to use the P-P and P-SV true amplitude reflectivities for AVO analysis.

### **Synthetic Data Study**

Synthetic data were used to test the 3-component processing flow for true amplitude recovery. The criterion for true amplitude recovery is that each process (particularly wavefield separation and waveshaping deconvolution) must retain the correct relative amplitude between the downgoing P wavefield and upgoing P and SV wavefields. If this criterion is met then the ratio of the downgoing P wavefield to the upgoing P and SV wavefields will be the true reflection amplitude. The synthetic data set was generated from the velocity model shown in Figure 4. The model is a gas-saturated sandstone encased in shale. The top of the sand is at 850 m and the base of the sand is at 1000 m. 11 levels were modeled between depths of 745 m and 845 m for offset positions of 50 m, 200 m, 400 m, and 600 m. The data were generated by ray tracing and convolution with a 35 Hz zero phase wavelet. The result of processing these data is the P-wave and S-wave gathers (Figure 5). To test the processing flow for true amplitude recovery, the amplitudes from the top of the sand reflection were picked and plotted along with the theoretical Zoeppritz equation solution for the interface versus P-wave angle of incidence (Figure 6). There is reasonable agreement between the processed data amplitudes and the theoretical amplitudes showing that the processing flow extracts amplitudes quite accurately from multioffset VSP data.

### **Field VSP Processing**

The results of the synthetic data study suggest that the multioffset VSP data can be processed for true amplitudes using the processing flow outlined in Figure 3. The first step is to rotate the horizontal channels into the radial (in the source-receiver plane) and the transverse (perpendicular to the source-receiver plane) directions. The radial and vertical channels of the 1250 m offset are shown in Figure 7. The P-wave direct arrival is on both channels and there are relatively strong P-SV mode-converted downgoing SV waves on the radial channel.

Following the horizontal rotations the vertical and radial channels are separated into the four modes of propagation; the downgoing P wavefield, the upgoing P wavefield, the downgoing S wavefield, and the upgoing S wavefield. The separation was accomplished using a parametric inversion technique developed by Esmersoy (1990), and Leaney (1990). In the parametric inversion the data are modeled as a superposition of a P wave and an SV wave. The local P and S velocities, angles of incidence, and waveforms are the model parameters. A least squares match between the observed data and model-generated data is used to estimate the model parameters. An example of the wavefield separation is shown in Figure 8 for the 1250 m offset. The data are now separated into the four modes of propagation of which the downgoing P wavefield and the upgoing wavefields will be used in further processing.

After wavefield separation the downgoing P wavefield is trace balanced (normalized) to correct for propagation losses along the downward path. The upgoing wavefields are then deconvolved using the downgoing P wavefield to design the

deconvolution operator. The downgoing P waves are trace balanced before deconvolution so the deconvolution operator does not introduce any spurious amplitude effects into the data. The upgoing wavefields are then trace balanced using the same factors used to trace balance the downgoing P wavefield; again this is to keep the correct relative amplitudes between the upgoing and downgoing wavefields. The data are then corrected for NMO using a ray-trace based NMO recovery routine using the velocity model from the P- and S-wave traveltimes. The NMO corrected data before waveshaping deconvolution are shown in Figure 9, and the NMO corrected data after waveshaping deconvolution are shown in Figure 10 for comparison. The deconvolution operator has worked well on the P wavefield, but it has introduced some ringiness into the upgoing S wavefield. There are several reasons that may explain the lower quality upgoing S wavefield. The upgoing S wavefield can be complicated by P-S mode converted transmissions reflecting as S waves (P-S-S) and interfering with the P-S reflections (Geis et al., 1990). Thus the complexity of the upgoing S wavefield may contribute to the lower quality P-S reflections. Another possibility is that the lower quality S wave data may be caused by poor geophone coupling in the horizontal direction.

After NMO correction each P-P and P-SV NMO corrected VSP is stacked and normalized by the average amplitude of the downgoing P wavefield at each offset position. So, there is now one P wave and one S wave true amplitude reflectivity trace for each offset position of the multioffset VSP. The data are stacked under the assumption that the P-wave angle of incidence changes little over the 11 levels of the VSP. This assumption is valid when the geophone levels are close to the interface. The purpose of stacking the data is to increase the signal to noise ratio. After the data are stacked, the traces are gathered into the P-wave and S-wave gathers (Figure 11). These gathers show the true bandlimited reflectivity as a function of offset.

The amplitudes for the events labeled in Figure 11 are plotted versus P-wave angle of incidence in Figure 12 and Figure 13. The P-wave angles of incidence were determined by ray tracing using the velocity model from the P- and S-wave traveltimes inversions. The P-P amplitudes are contaminated with some noise, but they do show a slight decrease in amplitude with offset. The P-S amplitudes are noisier, however they do show a slight increase in amplitude with offset as expected.

## DATA ANALYSIS AND FORWARD MODELING

The P- and S-wave gathers show the true seismic AVO response of the gas-bearing carbonate zone. The inverse problem is to use the amplitudes in these gathers to obtain an estimate of the  $V_p/V_s$  ratio in the gas-filled zone. A forward modeling approach was used to analyze the amplitudes in the gathers.

Along with the VSP, several other borehole measurements were acquired. A full-waveform sonic log and a bulk density log are two directly related to seismic reflection amplitudes. These measurements were used as inputs to the forward model. The logs were blocked with the constraint that the output blocked logs (Figure 12) contain the minimum number of interfaces necessary to reproduce faithfully the spectrum of the input logs within a given bandwidth (Carron, 1987). This technique was chosen because it is automatic, and the results could not be biased by the interpreter's expectations.

The inputs into the forward model are the blocked logs in the zone of interest, and the VSP interval velocities above the zone of interest. A ray-tracing algorithm was used to obtain the time reflectivity series. The reflectivity series was convolved with the waveshaping-deconvolved downgoing P wavefield (the recorded seismic wavelet), and then corrected for NMO, resulting in the P- and S-wave synthetic gathers (Figure 13). The downgoing P wavefield was used to maintain a consistent wavelet between the real and modeled data.

A comparison of real and forward modeled P-P amplitudes for the reflections from the top and base of the porous zone is shown in Figure 14 for the P-P reflections and Figure 15 for the P-SV reflections. Also plotted are the theoretical Zoeppritz equation curves for the respective interfaces. There is a good correlation between the forward-modeled amplitudes and the real-data amplitudes. The irregularities that do exist between the real and forward-modeled data can be attributed to noise, as the overall match is good, and the mismatches occur at the same P-wave angle of incidence (same offset position). The poor correlation between the theoretical (Zoeppritz equation) curves and the real and synthetic data points are an interesting result of this study. This poor correlation can be attributed to the limited bandwidth of the seismic data and the thin bed nature of the gas bearing zone.

The measured P-P reflections from the top of the porosity (Figure 14) are higher amplitude than the Zoeppritz equation amplitudes. This suggests that there is constructive wavelet interference for this event. The measured P-P reflection from the base of the porosity (Figure 14) and the measured P-S reflections (Figure 15) are all lower amplitude than the theoretical curves suggesting that there is destructive wavelet interference at these events. Thus for this case, single interface AVO analysis does not adequately describe the AVO behavior of the gas bearing zone, and complete multilayer modeling is necessary.

## CONCLUSIONS

The multioffset-VSP geometry is an effective AVO technique. Processing multioffset VSP data using a 3-component processing flow can recover the true reflection coefficients of seismic reflections by calculating the amplitude ratio of the incident to reflected waves. Full multilayer modeling was required to match the AVO response of the gas-bearing carbonate zone. In this case, single interface AVO analysis was not adequate.

## ACKNOWLEDGEMENTS

The first author was employed by Schlumberger of Canada during much of this work. We would also like to acknowledge the Perry Katopodis and Bharat Kapur of Schlumberger of Canada and the CREWES Project for their support and advice during the duration of this study.

## FUTURE WORK

Future work using this VSP geometry will be to use both the P-P and P-SV reflectivities in an AVO inversion. Using the additional information of the P-SV reflectivities should result in a better constrained inversion for the elastic parameters.

## REFERENCES

- Aki, K., and Richards, P.G., 1980, Quantitative seismology: Theory and methods, V.1: W.H. Freeman and Co.
- Carron, D., 19987, Optimal layer definition by simultaneous VSP inversion and log squaring: Presented at 57th Ann. Int. Mtg. Soc. Expl. Geophys.
- Chacko, S., 1990, Porosity identification using amplitude variations with offset: examples from South Samatra: *Geophysics*, 54, 942-951.
- Dankbaar, J.W.M., 1987, Vertical seismic profiling separation of P and S waves: *Geophys. Prosp.*, 35, 803-814.
- Esmersoy, C., 1990, Inversion of P and SV waves from multicomponent offset vertical seismic profiles: *Geophysics*, 55, 39-50.
- Gaiser, J.E., DiSiena, J.P., and Fix, J.E., 1984, VSP: Fundamentals of the downgoing wavefield and applications that improve CDP data interpretation, in Toksoz, N.N., and Stewart, R. R., Eds., *Vertical seismic profiling Part B: Advanced concepts*: Geophysical Press.
- Geis, W.T., Stewart, R.R., Jones, M.J., and Katapodis, P.E., 1990, Processing, correlating, and interpreting converted shear waves from borehole data in southern Alberta: *Geophysics*, 55, 660-669.
- Jolly, R.N., 1953, Deep-hole geophone study in Garvin County, Oklahoma: *Geophysics*, 18, 662-670.
- Koefoed, O., 1955, On the effect of Poisson's ratios of rock strata on the reflection coefficients of plane waves: *Geophys. Prosp.*, 3, 381-387.
- \_\_\_\_\_, 1962, Reflection and transmission coefficients for plane longitudinal incident waves: *Geophys. Prosp.*, 10, 304-351.
- Lee, M.W., and Balch, A.H., 1983, Computer processing of vertical seismic profile data: 48, 272-287.
- Leany, S.W., 1990, Parametric wavefield decomposition and applications: Presented at 60th Ann. Int. Mtg. Soc. Expl. Geophys.
- Mazzotti, A. and Mirri, S., 1991, An experience in seismic amplitude processing: *First Break*, 9, 65-73.
- Muskat, M. and Meres, M.W., 1940, Reflection and transmission coefficients for plane waves in elastic media: *Geophysics*, 5, 149-155.
- Ostrander, W.J., 1984, Plane wave reflection coefficients for gas sands at non normal angles of incidence: *Geophysics*, 49, 1637-1648.
- Rutherford, S.R., and Williams, R.H., 1989, Amplitude-versus-offset variations in gas sands: *Geophysics*, 54, 680-688.
- Stewart, R.R., and DiSiena, J.P., 1989, The values of VSP in interpretation: *The Leading Edge - Geophys.*, 8, 16-23.
- Stewart, R.R., Huddleston, P.D., and Kong Kan, T., 1984, Seismic versus sonic velocities: a vertical seismic profiling study: *Geophysics*, 49, 1153-1168.
- Tatham, R.H., and Krug, E.H., 1985, *Vp/Vs Interpretation: Developments in Geophysical Methods - 6.*, Ed. A.A. Fitch, Elsevier Applied Science Publications, London, New York.
- Widess, M.B., 1973, How thin is a thin bed?: *Geophysics*, 38, 1176-1180.

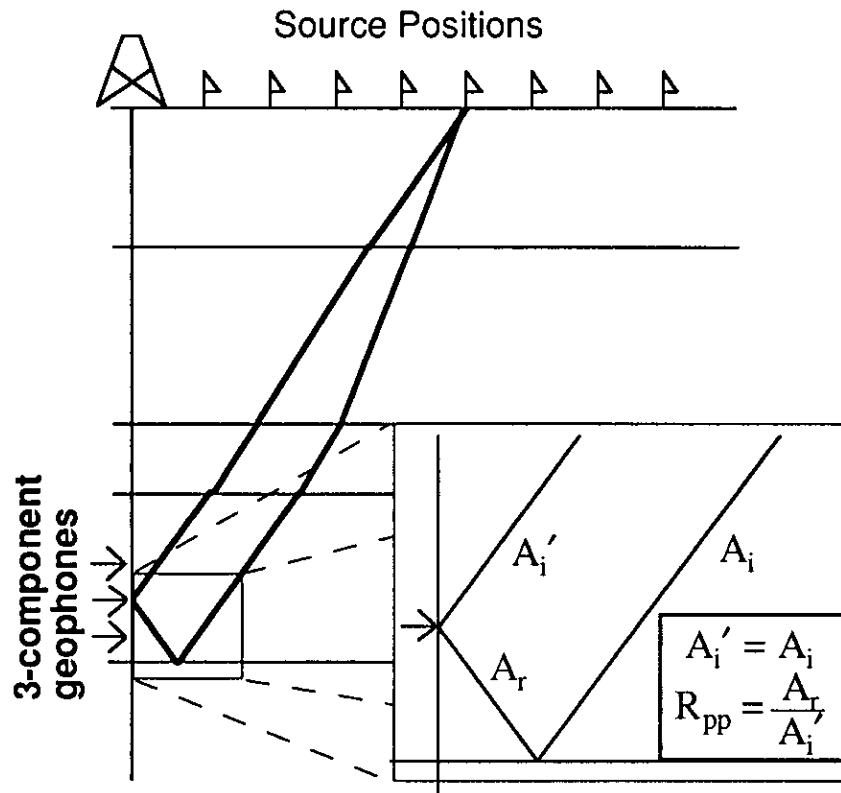


FIG. 1. Multioffset (walkaway) AVO VSP geometry showing source and receiver positions.

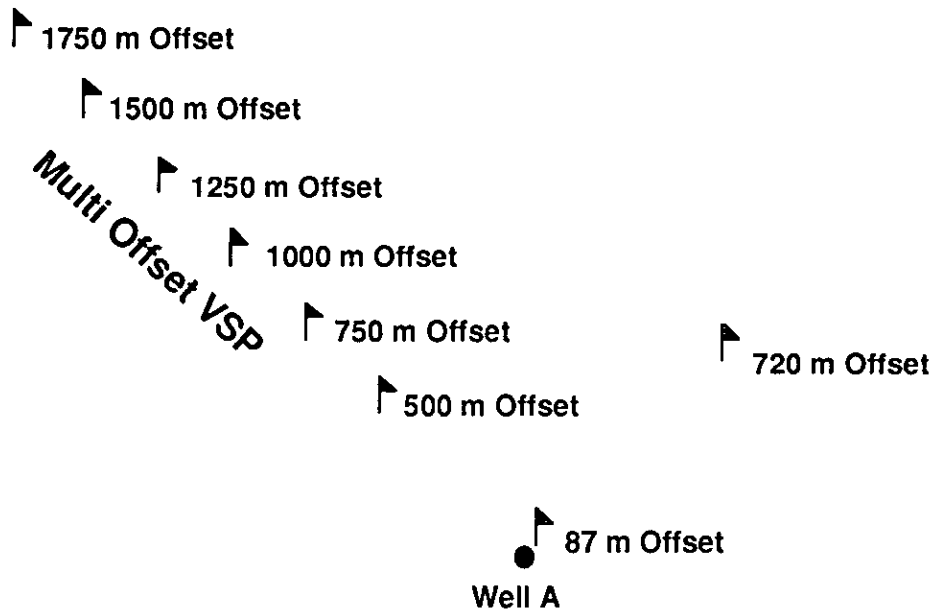


FIG. 2. Field VSP survey geometry.

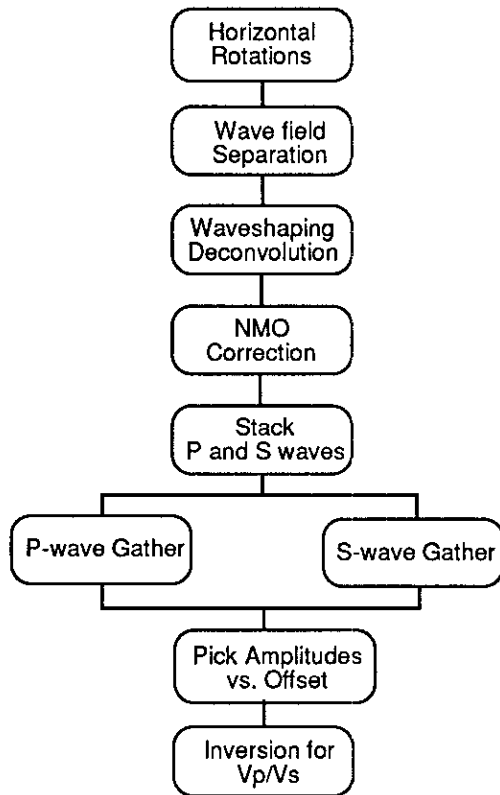


FIG. 3. 3-component processing flow.

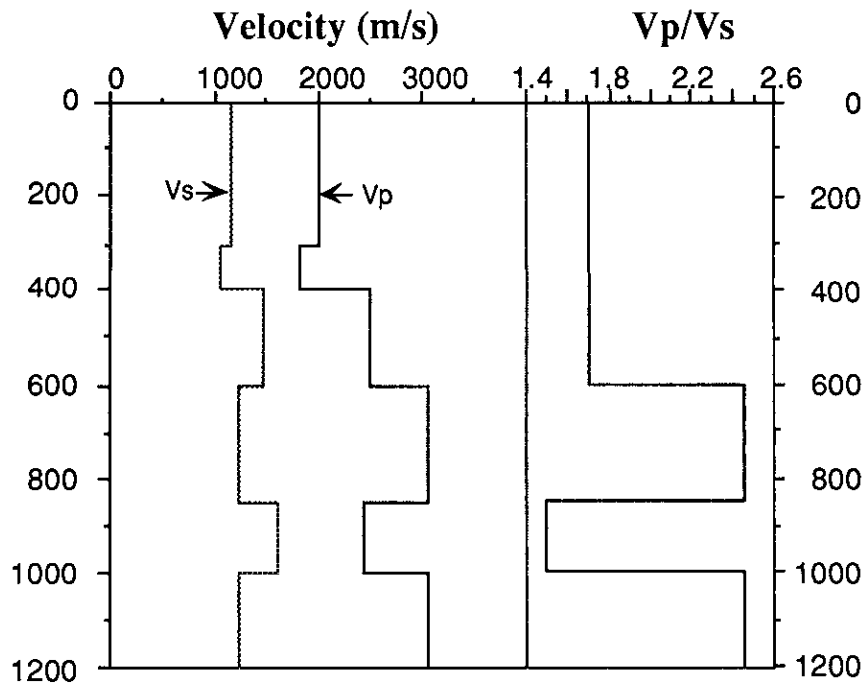


FIG. 4. Velocity model used to generate synthetic multioffset VSP. Source positions were at 50 m, 200 m, 400 m, and 600 m, eleven receivers were located between depths of 745 m and 845 m.

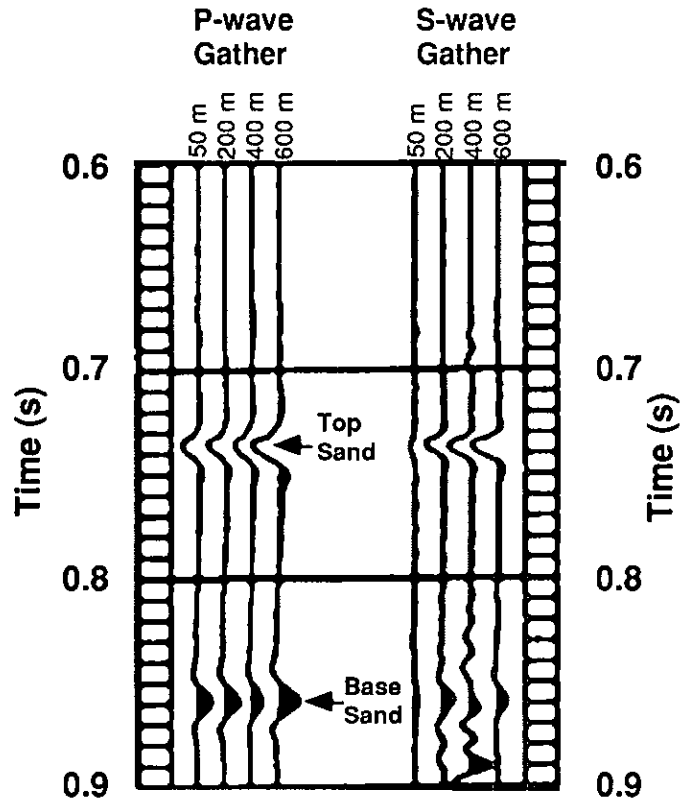


FIG. 5. Synthetic P- and S-wave gathers.

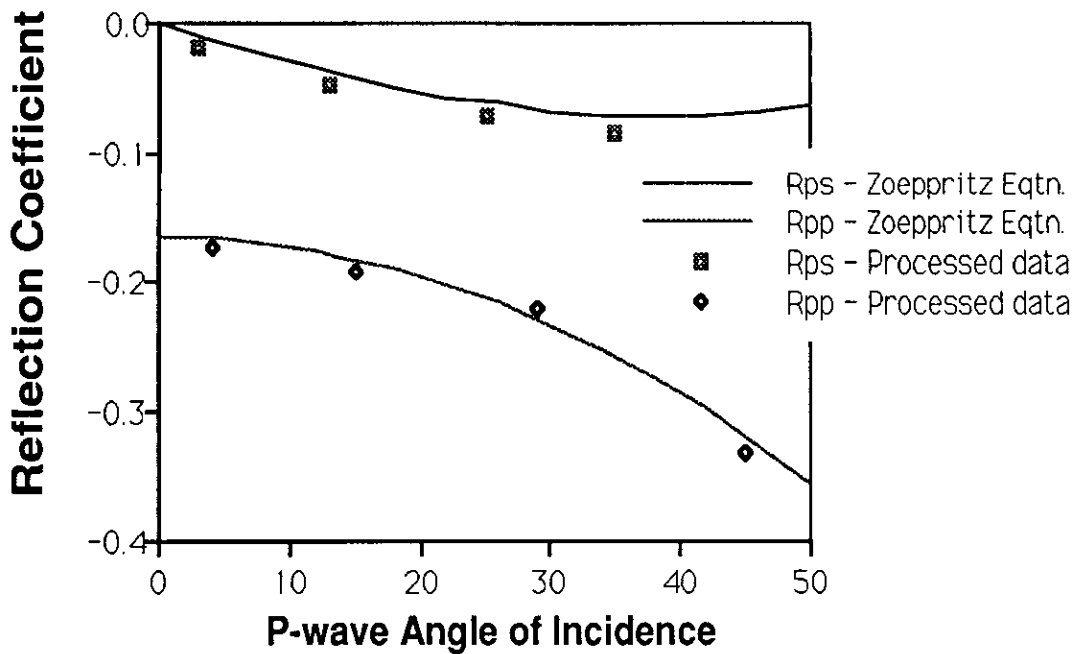


FIG. 6. Picked amplitudes from the top of the sand event and theoretical Zoeppritz equation curves for the interface.

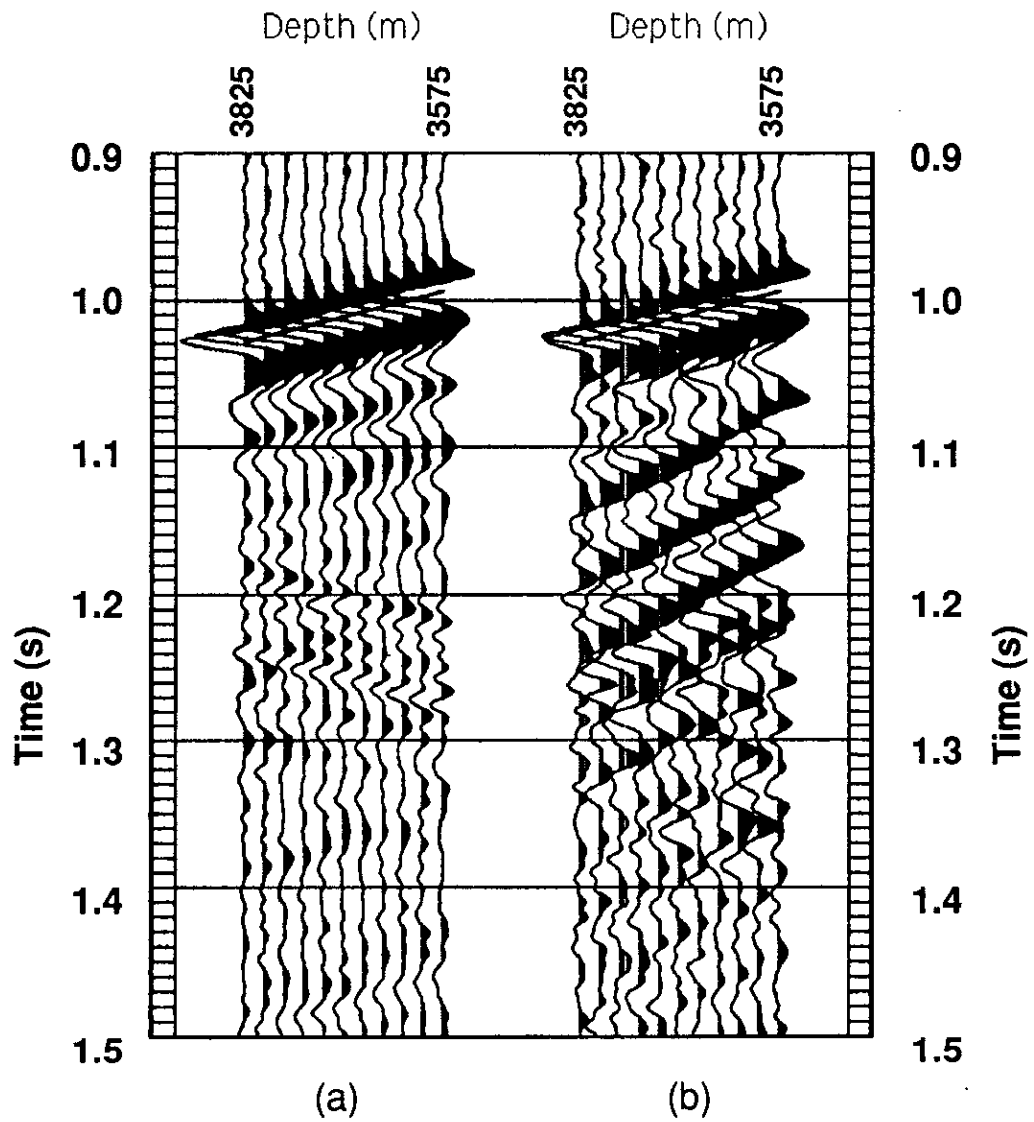


FIG. 7. (a) Raw vertical and (b) horizontal channels of the 1250 m offset of the walkaway VSP.

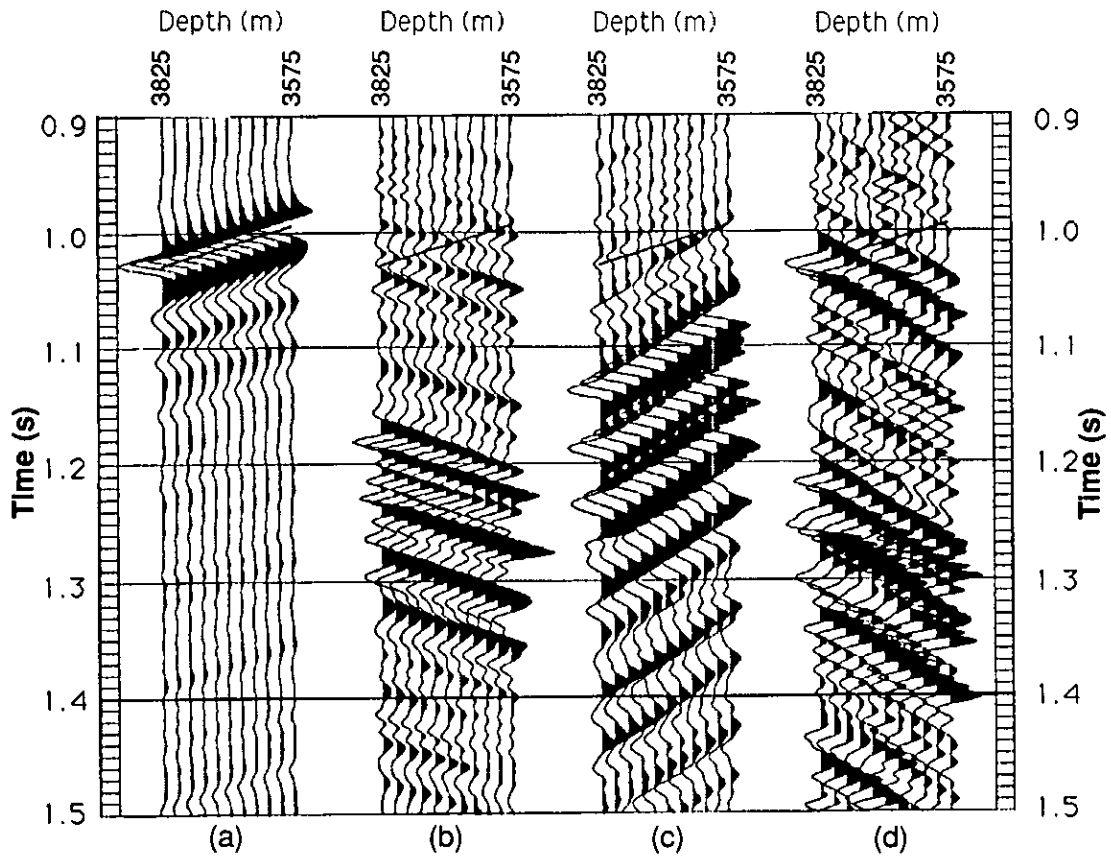


FIG. 8. Output of wavefield separation, (a) downgoing P wavefield, (b) upgoing P wavefield, (c) downgoing S wavefield, and (d) upgoing S wavefield.

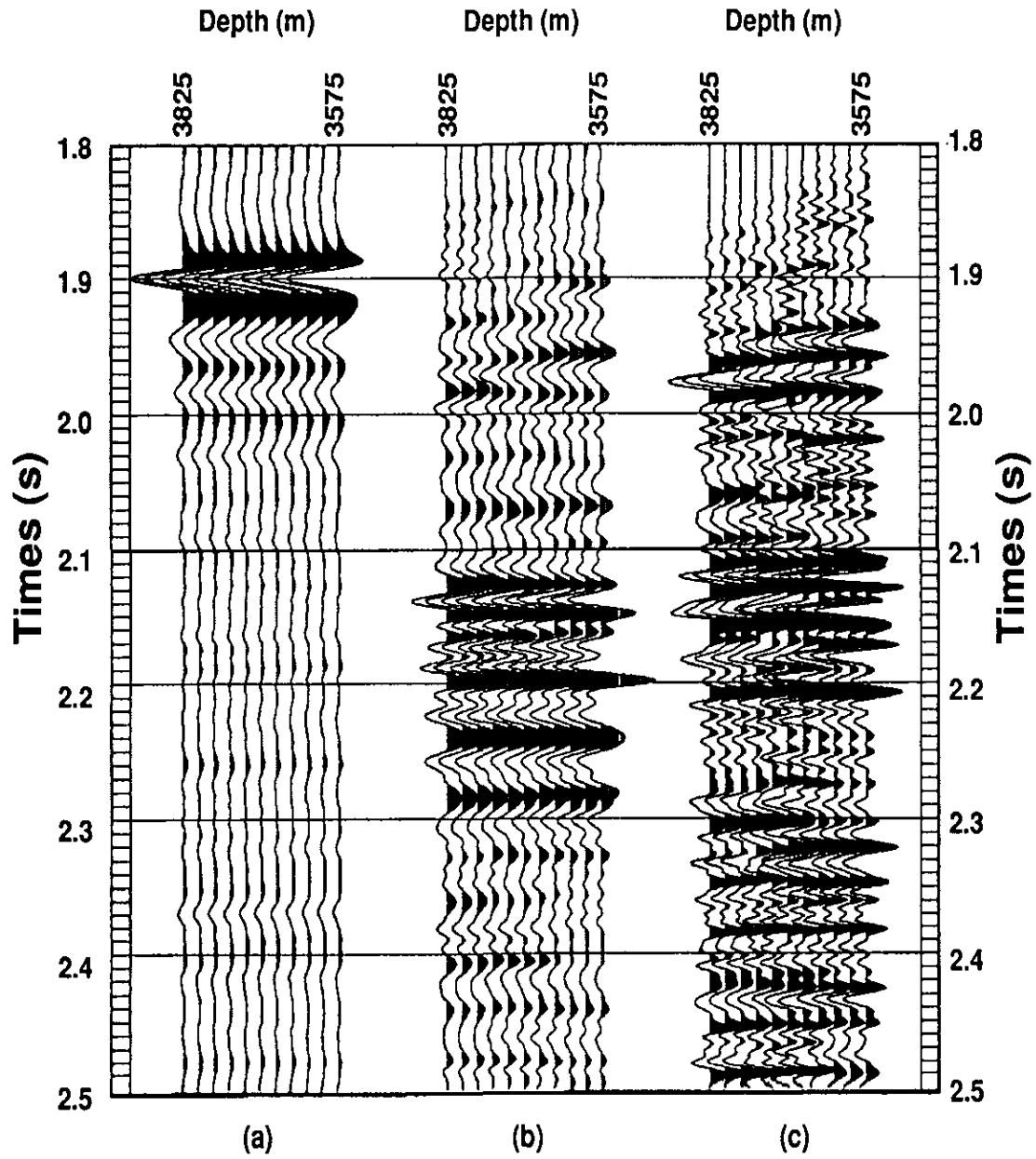


FIG. 9. (a) Flattened downgoing P wavefield, (b) NMO corrected upgoing P wavefield, (c) NMO corrected upgoing S wavefield before waveshaping deconvolution.

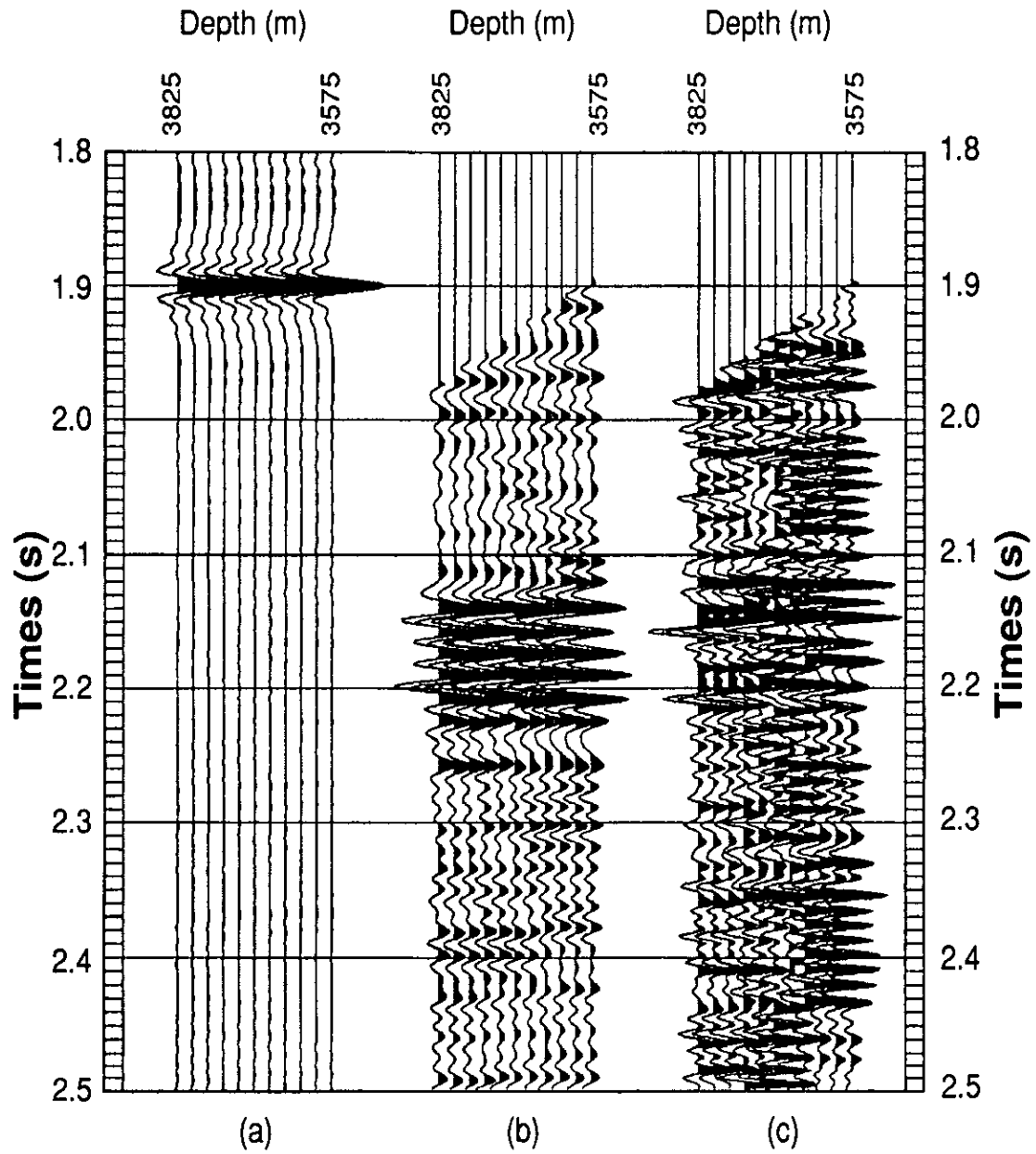


FIG. 10. (a) Flattened downgoing P wavefield, (b) NMO corrected upgoing P wavefield, (c) NMO corrected upgoing S wavefield after waveshaping deconvolution.

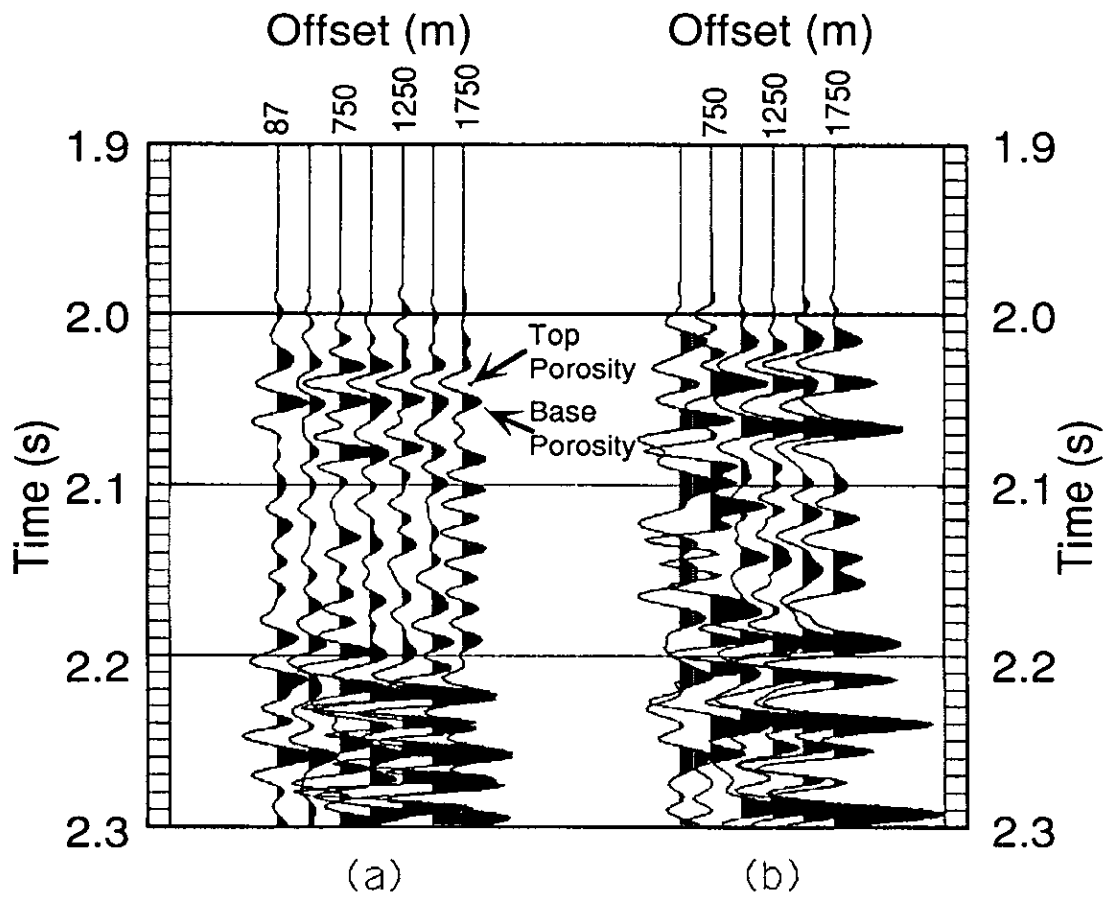
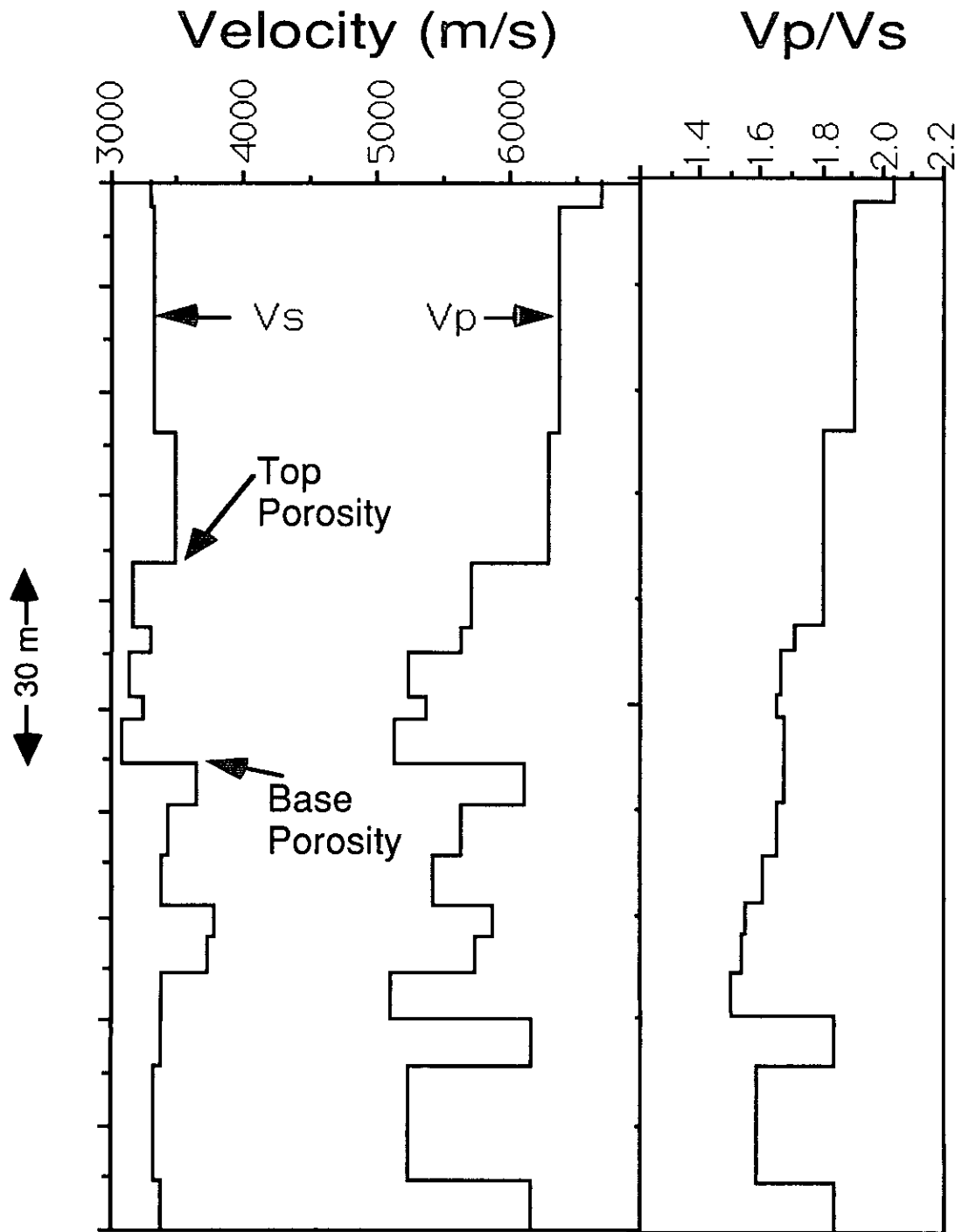


FIG. 11. (a) Processed P-wave gather, (b) processed S-wave gather.

FIG. 12. Blocked logs and  $V_p/V_s$  ratio.

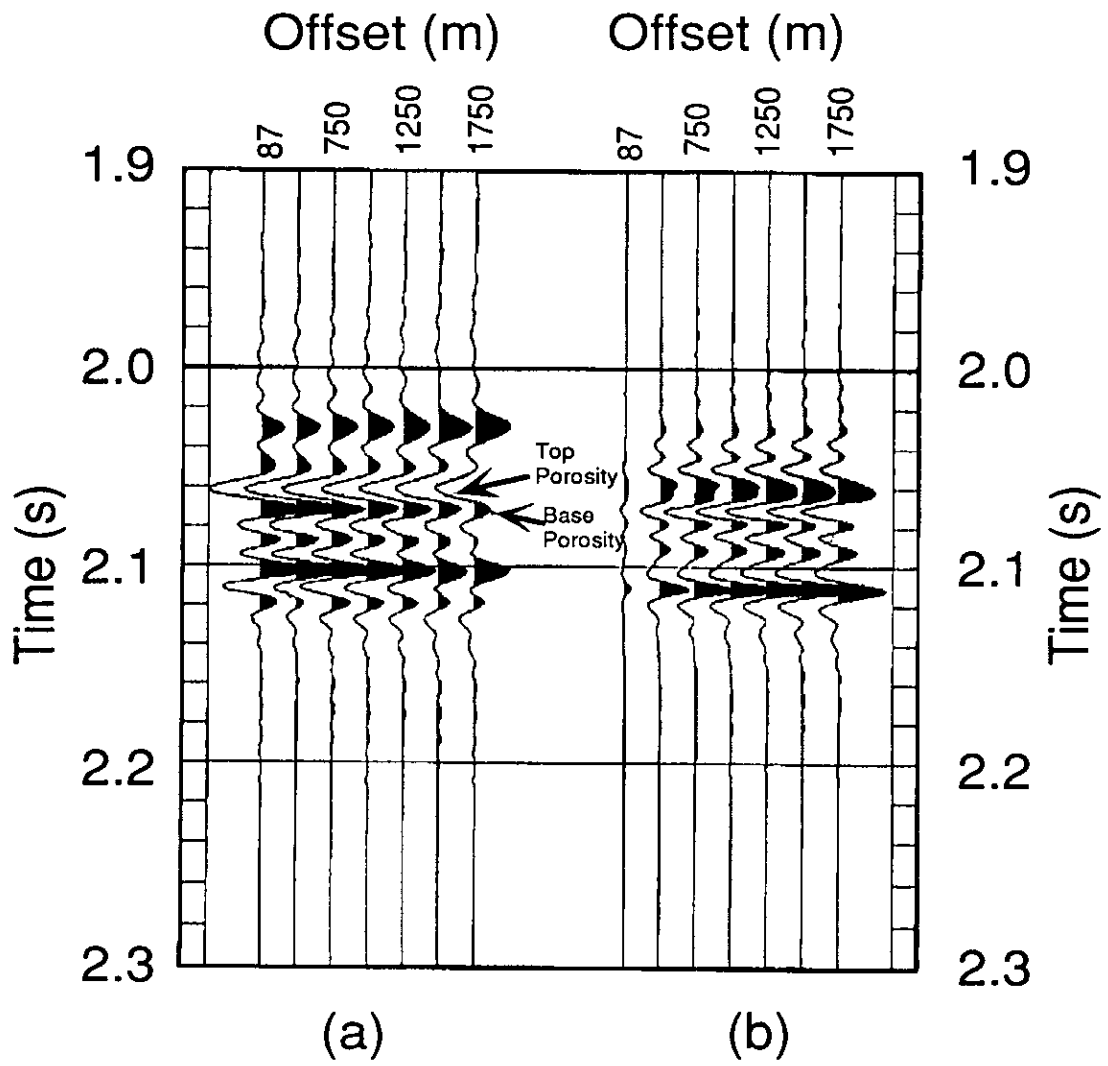


FIG. 13. Synthetic (a) P-wave gather, (b) S-wave gather.

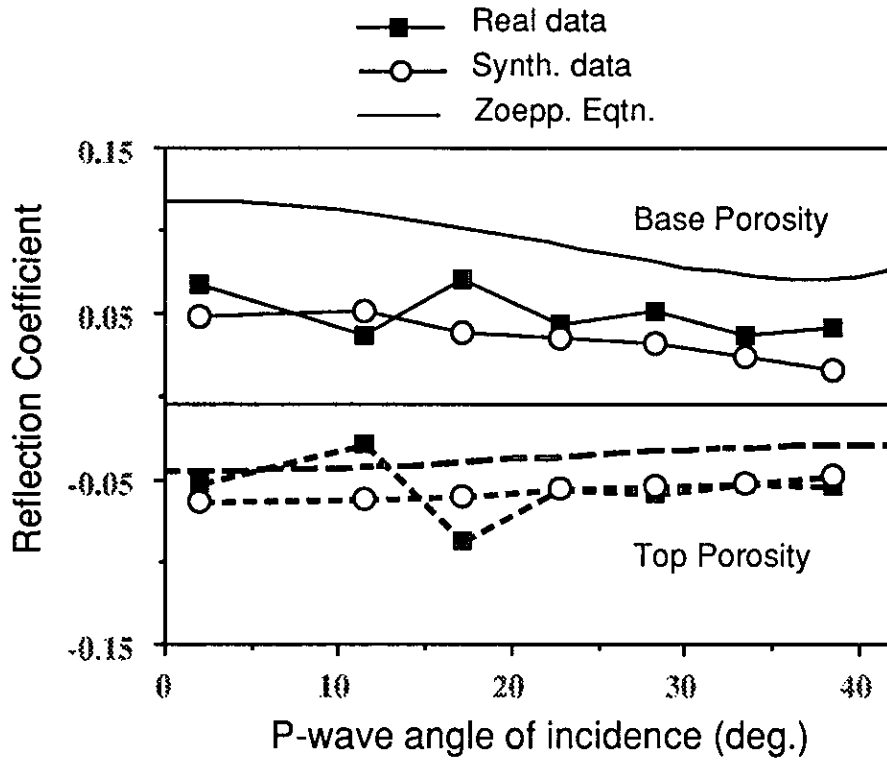


FIG. 14. Picked amplitudes from P-P gathers and Zoeppritz equation curves.

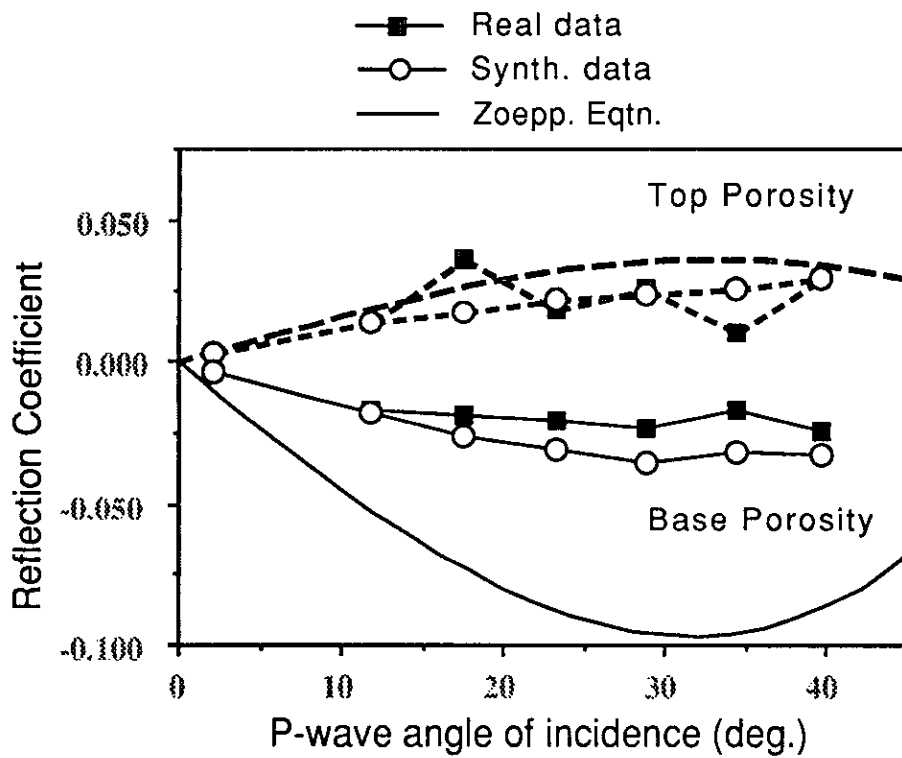


FIG. 15. Picked amplitudes from P-S gathers and Zoeppritz equation curves.